Redox Biology 34 (2020) 101498

Contents lists available at ScienceDirect

Redox Biology

journal homepage: www.elsevier.com/locate/redox

Hydrogen peroxide regulates endothelial surface N-glycoforms to control inflammatory monocyte rolling and adhesion

Kellie R. McDonald[a,b], Alexandria L. Hernandez-Nichols[a,b], Jarrod W. Barnes[c], Rakesh P. Patel[a,b,*]

[a] Department of Pathology, University of Alabama at Birmingham, Birmingham, AL, 35294, USA
[b] Center for Free Radical Biology, University of Alabama at Birmingham, Birmingham, AL, 35294, USA
[c] Department of Medicine, University of Alabama at Birmingham, Birmingham, AL, 35294, USA

ARTICLE INFO

Keywords:
N-glycosylation
Inflammation
Mannose
Mannosidase
Endoplasmic reticulum redox
Catalase
ICAM-1

ABSTRACT

Monocyte extravasation through the endothelial layer is a hallmark of atherosclerotic plaque development and is mediated by heavily N-glycosylated surface adhesion molecules, such as intercellular adhesion molecule-1 (ICAM-1). N-glycosylation is a key co- and post-translational modification that adds sugar molecules to Asparagine residues of surface and secreted proteins. While it has been suggested that surface and secreted proteins will not be expressed unless fully processed to a complex N-glycoform, emerging data has suggested that multiple N-glycoforms can exist on the cell surface. Previous data from our lab has shown that endothelial inflammation produces multiple N-glycoforms of ICAM-1, and that a hypoglycosylated, or high-mannose (HM), form of ICAM-1 enhances adhesion of pro-inflammatory monocytes associated with more severe atherosclerosis and adverse cardiac events. Despite these findings, little is understood about the regulation of N-glycans during disease. In this study, we focus on the α-mannosidases; an understudied class of enzymes for early N-glycan processing. We show that α-mannosidase activity decreases with TNFα treatment in endothelial cells, and this decrease correlates with HM N-glycan formation on the cell surface. Further, we demonstrate that this inhibition is class-I dependent, and is independent of NF-κB upregulation of ICAM-1. Finally, we show that this inhibition is due in part to hydrogen peroxide (H_2O_2), generated by Endoplasmic Reticulum oxidoreductase 1-α (ERO1α). These data provide insights into the regulation of surface N-glycans during inflammation and demonstrate a novel role for reactive species in N-glycan biosynthesis.

1. Introduction

N-glycosylation is a co- and post-translational modification that occurs on > 60% of surface and secreted proteins [1]. While in the endoplasmic reticulum (ER), proteins with the appropriate consensus sequence (Asn-X-Ser/Thr, where X ≠ Pro) are adorned with a tetradecasaccharide ($Glc_3Man_9GlcNac_2$) on the Asn residue via oligosaccharyltransferase (OST) [1]. As the protein is processed through the ER and Golgi, the tetradecasaccharide undergoes a series of enzymatic processing steps to trim and add new sugars, eventually resulting in a fully processed, or complex, N-glycoform; typically capped with sialic acids. This process is critical in protein folding and quality control mechanisms whereby incorrect or premature termination of N-glycan maturation triggers the unfolded protein response (UPR) resulting in protein degradation [2,3]. Fully processed N-glycoproteins are trafficked to the cell membrane where they participate in regulating cell-to-cell and cell-environment communication and signaling, or are secreted to perform function in the extracellular space [1,4–6].

While the accepted paradigm of N-glycosylation is that proteins must be fully processed to the complex N-glycoform before being expressed on the cell surface, we and others have identified under-processed, or high mannose (HM), surface N-glycan structures on the surface of inflamed or dysfunctional endothelial cells that characterize vascular inflammation associated with atherosclerosis or cancer [7–15]. Our recent data have identified the endothelial adhesion molecule, intercellular adhesion molecule 1 (ICAM-1) as one protein whose N-glycoforms are regulated during inflammation. Specifically, we showed that inflammatory stimuli, including TNFα or oscillatory flow, induce expression of both HM and complex N-glycoforms of ICAM-1 on the cell surface [10,16]. Further, we demonstrated that HM-ICAM-1 may be the predominant N-glycoform to selectively regulate adhesion of non-classical/intermediate ($CD14^+CD16^+$) or pro-inflammatory monocytes that strongly associate with atherosclerosis disease severity [15,17–19]. HM-ICAM-1 did not mediate adhesion of classical ($CD14^+CD16^-$)

* Corresponding author. Department of Pathology, University of Alabama at Birmingham, 901 19th St. South, BMRII 532, Birmingham, AL, 35294, USA.
E-mail address: rakeshpatel@uabmc.edu (R.P. Patel).

https://doi.org/10.1016/j.redox.2020.101498
Received 19 February 2020; Received in revised form 2 March 2020; Accepted 4 March 2020
Available online 06 March 2020

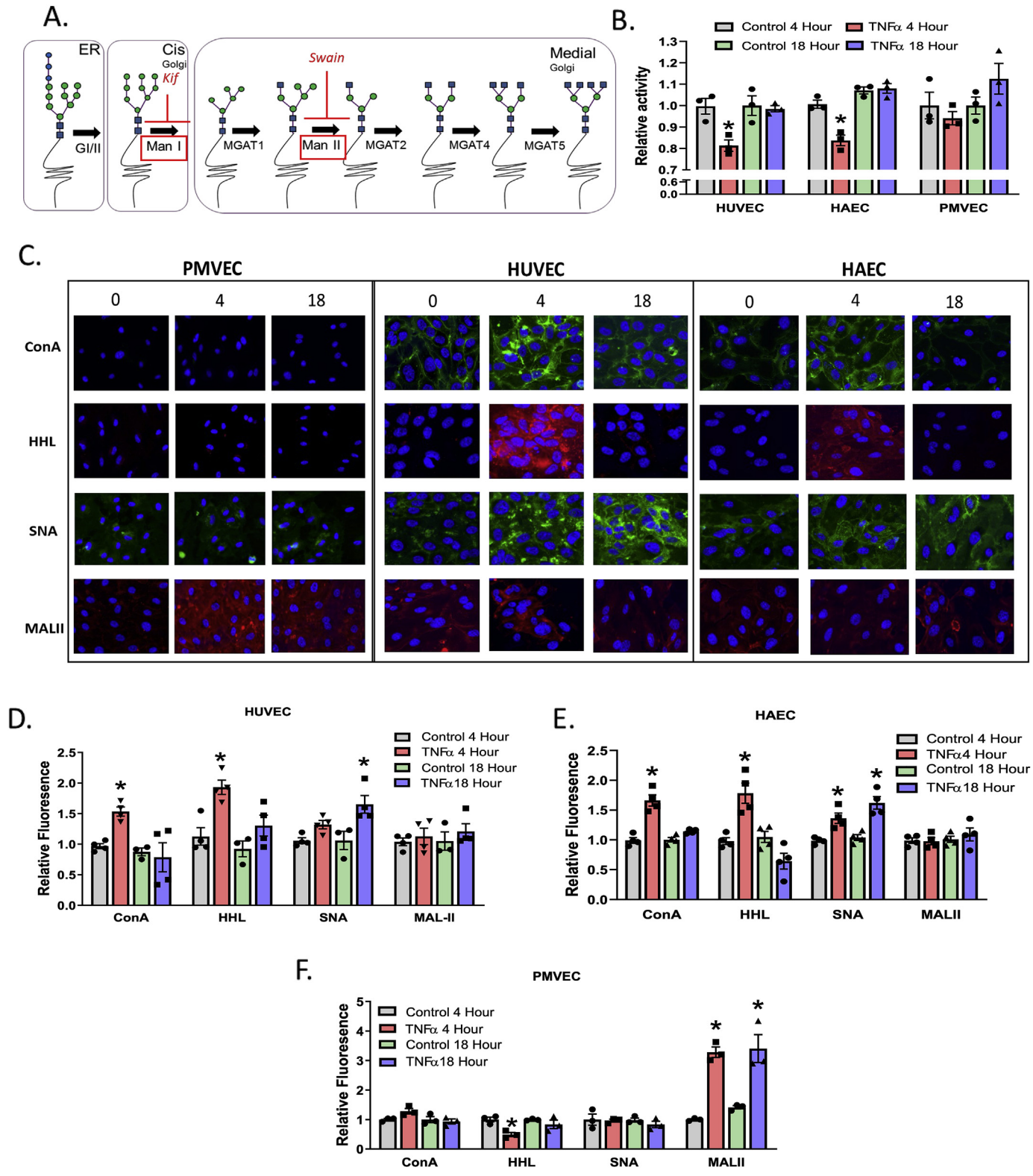

Fig. 1. TNFα inhibits α-mannosidase activity and in parallel increases HM N-glycan structures on the cell surface. A. Schematic of N-glycan biosynthesis and location of α-mannosidase enzymes highlighted in red boxes with sites of Kif and Swain inhibition indicated. **B.** Relative α-mannosidase activity in HUVECs, HAECs, and PMVECs after TNFα treatment. * = $p \leq 0.05$ compared to respective controls by one-way ANOVA with Tukey's post-test. Data are mean ± SEM, n = 3. **C.** Representative images of lectin staining across cell lines treated with TNFα for 0, 4, and 18 h. Green (ConA and SNA) and red (HHL and MAL-II) represent positive lectin staining. Blue staining is a DAPI nuclear stain. **D – F.** Relative fluorescence of lectin binding measured by ELISA. * = $p \leq 0.05$ compared to respective controls per lectin. Data are mean ± SEM, n = 3–4. (For interpretation of the references to colour in this figure legend, the reader is referred to the Web version of this article.)

monocytes, suggesting distinct endothelial N-glycoforms are important in mechanisms regulating how different leukocyte subsets traffic to specific sites of inflammation. The molecular mechanism(s) that control formation of distinct ICAM-1 N-glycoforms remains are not known.

N-glycan biosynthesis occurs via a linear pathway, suggesting that inhibition of enzymes catalyzing early steps of trimming mannose residues would lead to the accumulation of HM-N-glycans on newly translated proteins (Fig. 1A). Mannose trimming is catalyzed by class I and class II α-mannosidases [1,2]. Class I α-mannosidases are expressed in both the ER and Golgi and sequentially cleave terminal α-1,2 mannose linkages on 9-mannose structures (HM) to form 5-mannose hybrid structures [20–24]. Class II α-mannosidases exist in the Golgi, cleaving terminal α-1,3 and α1,6 mannose linkages on 5-mannose hybrid structures to form 3-mannose complex structures [20,23,25] (Fig. 1A). Our previous work has shown that TNFα inhibits total (class I plus class II) α-mannosidase activity in endothelial cells but the mechanisms underlying this effect remain unclear [10,26]. In this study, we demonstrate that inhibition of α-mannosidases by TNFα is class-I dependent, is independent of NF-κB upregulation of ICAM-1, and occurs by an endoplasmic reticulum oxidoreductase 1 – alpha (ERO1-α) generated hydrogen peroxide (H_2O_2) dependent mechanism. These data suggest a novel role for ER-redox signaling in controlling protein N-glycoforms and cell surface and secreted protein function.

2. Methods

2.1. Materials

Human umbilical vein endothelial cells (HUVEC) were isolated from umbilical veins via collagenase as described [7] and according to UAB Institutional Review Board approved protocols. Human aortic endothelial cells (HAEC) and pulmonary microvascular endothelial cells (PMVEC) were purchased from ATCC (Manassas, VA). MCDB131, HI-FBS, trypsin, L-glutamine, and Penicillin/Streptomycin were purchased from Invitrogen (Carlsbad, CA). *Concanavalin A* (ConA), *Sambucus Nigra* (SNA), *Hippeastrum Hybrid Amaryllis* (HHL), and *Maackia Amurensis Lectin II* (MAL-II) lectins were purchased from Vector laboratories (Birlingame, CA). Kifunensine (Kif), Swainsonine (Swain), and EUK134 were purchased form Cayman Chemicals (Ann Arbor, MI). EN460 was purchased from Millipore-Sigma (Burlington, MA). Resorufin α-D-mannopyranoside was purchased from Marker Gene Technologies (Eugene, OR). GKT137831 was a generous gift from Dr. Victor Thannickal (University of Alabama at Birmingham). Antibodies for ICAM-1 and ERO1α were from Cell Signaling Technologies (Danvers, MA) (4915 and 3264, respectively). All other reagents were purchased from Sigma-Aldrich (St. Louis, MO) unless otherwise noted.

2.2. Cell culture and treatment

HUVEC, HAEC, and PMVEC were cultured in 6 well plates as previously described [10] and used between passages 3–7 for experiments. Cells were used within one day of reaching confluence and were serum-starved in MCDB-131 media containing 1% FBS for 2 h prior to treatment. Cells pre-treated with the class I and II α-mannosidase inhibitors, Kif or Swain, respectively, for 2 h following serum starvation and prior to exposure to 10 ng/mL TNFα for 4 h, unless otherwise stated. Exogenous hydrogen peroxide concentration was measured at 240 nm and was diluted immediately prior to cell treatment. Pre-treatment with PEG-catalase or EN460 was done 30 min prior to TNFα treatment. Concentrations of different reagents are indicated on figure legends. EN460 and GKT were dissolved in DMSO with a final concentration of less than 0.5% DMSO in the well. Parthenolide and Swain were dissolved in EtOH and final concentrations were less than 1% EtOH in the well. All other reagents were dissolved in aqueous solutions.

2.3. α-mannosidase activity assay

Total (class I and II) α-mannosidase activity was determined utilizing three mannosidase substrates. Activity was measured as described [10] with Resorufin, 4-methylmumbelliferyl, or p-nitrophenyl α-D-mannopyranoside substrates with minor modifications. Cells were washed with PBS before lysis in PBS containing 1% Triton X-100 for 10 min on ice before clarification at 10,000 × *g* for 10 min 40 μL cell lysate (corresponding to 30–40 μg protein) was prepared, in a microtiter plate, in 100 mM acetate buffer (pH 6.5) and 200 μM of resorufin-α-D-mannopyranoside, 100 μM 4-methylmumbelliferyl α-D-mannopyranoside or 10 mM p-nitrophenyl was added to start the reaction. Assays with resorufin-α-D-mannopyranoside and 4-methylmumbelliferyl α-D-mannopyranoside were read every 5 min for 18 h at 37 °C, with mixing performed prior to each measurement, at 550/595 or 360/445, respectively, in a Biotek Synergy plate reader. At the end of an 18 h incubation, a basic stop solution (pH 10.4) was added to the reaction with *p*-nitrophenyl and absorbance was measured at 405 nm in a Biotek Synergy plate reader.

2.4. Western blotting

Cells were treated as described and lysed in RIPA buffer for 10 min on ice. A total of 20 μg protein was loaded onto a 10% SDS-PAGE gel, subjected to electrophoresis before being transferred to a 0.2 μm nitrocellulose membrane, and probed for the described protein by incubation with primary antibody overnight at 4 °C with rocking. Membranes were incubated with HRP-linked, species-appropriate secondary antibodies for 2 h at RT prior to chemiluminescence measurement. Images were analyzed using ImageQuant software (GE Healthcare Life Sciences).

2.5. Lectin staining

Cells were grown on gelatin-coated glass coverslips and treated as indicated. Cells were washed with ice cold 1x PBS containing 1 mM $MgCl_2$ and $CaCl_2$ before being incubated with 10 μg/mL FITC- or biotin-tagged lectins (ConA, HHL, SNA, MAL-II) for 10 min on ice. Cells were then fixed for 15 min at RT in 4% paraformaldehyde before being washed and mounted with DAPI-containing mounting medium. Cells treated with biotin-tagged lectins also underwent a 1 h incubation at RT with avidin conjugated to AlexaFluor 594 prior to DAPI mounting. Images were acquired on a Biotek Lionheart fluorescent microscope.

2.6. Surface ICAM-1 and lectin ELISAs

Cells were grown in 96-well plates and treated as described. Cells were then washed with ice cold 1x PBS containing 1 mM $MgCl_2$ and $CaCl_2$ before processing. For ICAM-1 surface staining, cells were fixed for 15 min at RT in 4% paraformaldehyde, followed by 1 h blocking in 5% normal serum. Cells were incubated with an ICAM-1 antibody (BMS108, ThermoFisher) overnight at 4 °C before incubation with a species-appropriate secondary antibody conjugated to AlexaFluor 594 for 1 h at RT. After washing, plates were read at 561/617 in a Biotek Synergy plate reader. To quantify lectin binding cells were incubated with 10 μg/mL biotin-tagged lectins (HHL, SNA, MAL-II) for 10 min on ice, then fixed for 15 min at RT in 4% paraformaldehyde before being washed. Cells were then incubated with avidin conjugated to AlexaFluor 594 for 1 h at RT and read on a plate reader at 561 nm (excitation) and 617 nm (emission).

2.7. ROS measurement

Cells were grown in 96 well plates and treated as described. After treatment, cells were washed with PBS and 10 μM DCFDA was added to each well for 60 min before being read on a plate reader at 485/535.

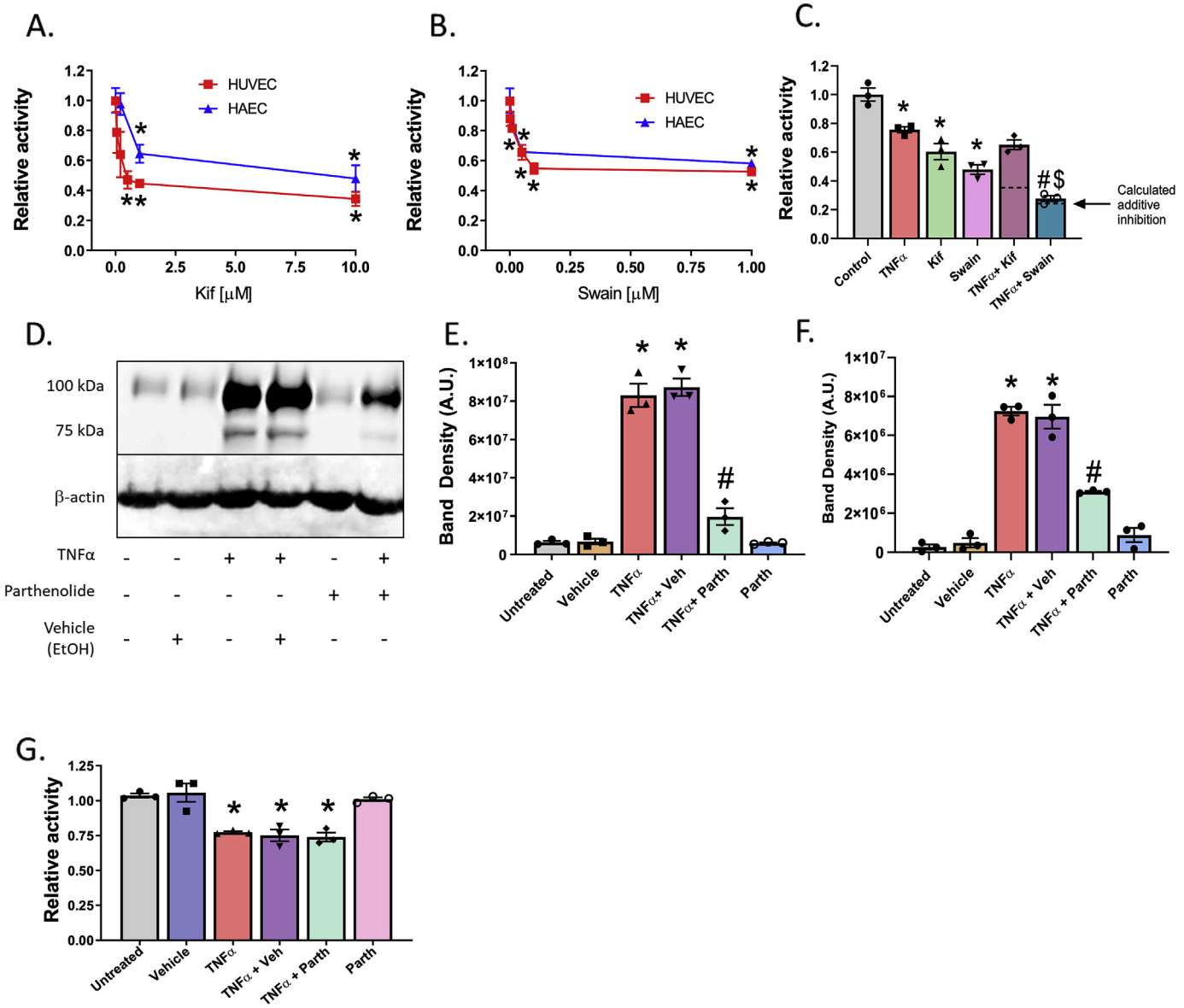

Fig. 2. TNFα inhibition of α-mannosidase activity is class-I dependent and independent of NF-κB. A. HUVECs and HAECs were treated for 2 h with increasing doses of Kif and total α-mannosidase activity measured. * = $p \leq 0.05$ compared to untreated cells by 1-way ANOVA with Tukey post-test relative to no Kif treatment. Data are mean ± SEM, n = 3. **B.** HUVECs and HAECs were treated for 2 h with increasing doses of Swain and total α-mannosidase activity measured. * = $p \leq 0.05$ compared to vehicle treated cells by 1-way ANOVA with Tukey post-test. Data are mean ± SEM, n = 3. **C.** HUVECs were pretreated with 1 μM Kif or Swain for 2 h prior to 4 h TNFα treatment and α-mannosidase activity measured. Dotted lines represent calculated additive effect determined by level of inhibition from TNFα combined with inhibition of Kif alone or Swain alone as described in results section.* = $p \leq 0.05$ compared to control; # = $p \leq 0.05$ compared to TNFα; $ = $p \leq 0.05$ compared to Swain alone by 1-way ANOVA with Tukey post-test. Data are mean ± SEM, n = 4. **D.** Western blot image and **E** & **F.** analysis of complex and HM-ICAM-1, respectively, in HUVECs pretreated with 5 μM Parth prior to 4 h TNFα treatment. * = $p \leq 0.05$ compared to control; # = $p \leq 0.05$ compared to TNFα by 1-way ANOVA with Tukey post-test. **G.** α-mannosidase activity measured in cells treated as described in **D** & **E.** * = $p \leq 0.05$ compared to untreated control by 1-way ANOVA with Tukey post-test. Data are mean ± SEM, n = 3.

2.8. Proximity-ligation assay

Proximity-ligation assay was performed using protocols that avoid permeabilization as described [15]. Briefly, 20 μg of the following biotinylated lectins: the HM and hybrid N-glycan-specific lectin, ConA; the α2,6-sialyation specific lectin, SNA; the HM-specific lectin, HHL; or the α2,3-sialylation specific lectin, MAL-II, were added for 30 min at 4 °C. These lectins were chosen to provide broad coverage of different N-glcyan structures. After washing twice with PBS, samples were blocked with 1X Carbo-Free blocking solution (Vector Labs) for 30 min at 20–25 °C. Immediately following blocking, samples were incubated with oligo-tagged avidin or *anti*-ICAM-1 (10 μg/mL) for 1 h at 37 °C followed by ligation and amplification steps as per the protocol.

Human ICAM-1 antibody (clone RR1/1) used recognizes an extracellular (domain 1) epitope on ICAM-1 that is devoid of N-glycans. Slides were left to dry and mounted using the DuoLink® mounting medium containing DAPI.

2.9. Monocyte isolation and adhesion assay

Primary human monocytes were isolated from freshly drawn whole blood collected by venipuncture from healthy volunteers using magnetic beads as described [15,16]. Briefly, after removal of the plasma layer, blood was layered on top of a Histopaque gradient, centrifuged,

and monocytes isolated from the top layer. Monocytes were incubated with a CD16 antibody and isolated using positive selection via a magnetic column. The flow-through ($CD16^-$ cells) was then incubated with a CD14 antibody to isolate distinct $CD16^+$ and $CD16^-$ monocyte populations. All cell separations were confirmed via flow cytometry analysis and protocols approved by the UAB Institutional Review Board. Monocyte populations were incubated with 1 μM fluorescent CellTracker™ dyes; $CD16^-$ cells were labeled with CellTracker™ green (CMFDA) and $CD16^+$ cells were labeled with CellTracker™ blue (CMAC). Monocytes were then were combined in equal amounts (final cell count 250,000 cells/mL; 125,000 cell/mL of each subtype), unless otherwise stated. Treated HUVEC were exposed to fluorescent monocytes at a flow rate of 100 μL/min, corresponding to 1 dyne/cm [2], in a GlycoTech parallel plate flow chamber. Images were captured on a Biotek Lionheart live cell imager over 2 min at 30 frames/sec. Any cell that was stationary for ≥5 s was considered firmly adhered as described bib27[16,27]. Rolling velocities (velocity of monocytes that are engaging with and rolling over the endothelium) were calculated from 5 random cells using the mTrackJ plugin on ImageJ (NIH).

2.9.1. Statistics

All statistical analysis was performed using GraphPad Prism software. Paired *t*-test or one-way ANOVA followed by Tukey's post hoc test were performed as indicated in the figure legends. Each experiment (> 3 replicates within each experiment) was performed at least three times, with means from each experiment providing a single replicate.

3. Results

3.1. TNFα inhibits α-mannosidase activity and increases hypoglycosylation in ECs in a time-dependent manner

HUVECs, HAECs, and PMVECs were exposed to 10 ng/mL TNFα for 0–18 h and α-mannosidase activity measured as described in methods. With HUVECs and HAECs, α-mannosidase activity was significantly decreased after 4 h, but rebounded back to control levels by 18 h (Fig. 1B). While the extent of inhibition appears to be modest (20–25%), the employed activity assay measures all class I and II α-mannosidases (total 9 isoforms) suggesting that not all isoforms of α-mannosidases are being inhibited. In PMVECs, TNFα had no significant effect on α-mannosidase activity at any time (Fig. 1B). To assess if inhibition of α-mannosidase activity translated to altered surface N-glycans, staining with ConA, HHL, SNA, and MAL-II lectins, specific for high-mannose (HM), hybrid, α−2,6- or α−2,3- sialylated N-glycans respectively, was performed. Fig. 1C shows representative images of lectin staining, with Fig. 1D–F showing quantitation of lectin binding using ELISA performed in parallel experiments. TNFα increased surface expression of HM structures in HUVECs and HAECs, but not PMVECs, at 4 h, with expression returning to basal level by 18 h paralleling changes in α-mannosidase activity. Notably, TNFα induced a significant increase in α−2,3-sialyation on the surface of PMVEC, but not other ECs tested (Fig. 1F).

3.2. TNFα inhibition of α-mannosidase activity is class-I dependent

There is currently no class-specific α-mannosidase activity assay; the assay used here measures both class I and II (total) α-mannosidase activity. To elucidate the distribution of class I and II α-mannosidases in ECs, activity was measured after treating HUVECs and HAECs with increasing doses of the α-mannosidase class I and II inhibitors, Kifunensine (Kif) and Swainsonine (Swain), respectively. Refer to Fig. 1A for Kif and Swain inhibition sites. In both ECs tested, Kif (Fig. 2A) and Swain (Fig. 2B) each inhibited α-mannosidase activity in a dose-dependent manner, with maximal inhibition of ~50–60% for class I and ~40–50% inhibition of class II, suggesting approximately equal distribution of each α-mannosidase activity in ECs.

Next, HUVECs were treated with Kif (1 μM) and Swain (1 μM) at doses that maximally inhibited each α-mannosidase prior to exposure to TNFα, and α-mannosidase activity measured. Fig. 2C shows that individually TNFα, Kif or Swain inhibited α-mannosidase activity by ~25%, ~40%, and ~50%, respectively. When combined, TNFα and Swain inhibited α-mannosidase activity ~70% similar to the calculated additive inhibitory effects determined by combining the inhibitory effects of TNFα and Swain alone (indicated by dotted line). The combination of TNFα and Kif did not lead to a further inhibition beyond each alone (if additive, calculated combined effect should ~~65% inhibition) suggesting that TNFα inhibits class I α-mannosidase activity.

To assess mechanism(s), we first tested whether TNFα-dependent inhibition involved NF-κB, which is known to be activated and mediate upregulation of ICAM-1 and other adhesion molecules [8,28–30]. HUVECs were treated with TNFα with or without the NF-κB inhibitor, Parthenolide (Parth), and expression of ICAM-1 determined by Western blotting (Fig. 2D). TNFα induced ICAM-1 expression indicated by two bands, at ~75 KDa and ~100 KDa, which we have shown correspond to HM- and α-2,6-sialylated complex ICAM-1 N-glycoforms [10]. Parthenolide inhibited expression of both complex ICAM-1 and HM-ICAM-1 by ~60–80% (Fig. 2E and F). Fig. 2G shows that parthenolide had no effect on TNFα dependent inhibition of α-mannosidase activity however. These data together suggest that α-mannosidase activity is inhibited in parallel with, but independent of, NF-κB-dependent protein upregulation.

3.3. H_2O_2 inhibits class-I α-mannosidase activity

We hypothesized that H_2O_2 may mediate TNFα-dependent inhibition of α-mannosidase activity. Fig. 3A shows that augmenting cellular catalase activity using PEG-catalase prevented TNFα dependent inhibition of α-mannosidase activity. Notably, PEG-catalase alone, in the absence of TNFα further increased α-mannosidase activity above baseline. Data shown in Fig. 3B demonstrates that exogenous H_2O_2 inhibited α-mannosidase activity in a dose- and time-dependent manner. At each dose, maximal inhibition occurred within 10 min. Activity returned to control levels within 30 and 60 min for 1 and 10 μM H_2O_2 respectively, but stayed inhibited over 1 h with the 100 μM H_2O_2 (Fig. 3B).

Finally, to determine which class of α-mannosidases H_2O_2 was inhibiting, ECs were pre-treated with Kif or Swain prior to H_2O_2 exposure. Consistent with the effects of TNFα, H_2O_2 inhibited class I activity, as demonstrated by the additive inhibition seen when pre-treated with Swain (Fig. 3C). No additive effect was seen when pretreated with Kif; dotted lines represent the expected inhibitory effect if additive.

3.4. Role of H_2O_2 in regulating HM-ICAM-1 formation and non-classical monocyte adhesion

Having established a role for endogenous H_2O_2 in mediating inhibition of α-mannosidase activity, next we determined H_2O_2 regulates ICAM-1 N-glycoform expression and in turn pro-inflammatory monocyte rolling and adhesion. Fig. 4A shows that PEG-catalase prevented TNFα-dependent increases in surface HM/hybrid N-glycans, but had no effect on complex α-2,6-sialyated N-glycans (SNA binding). No changes in α-2,3-sialyated N-glycans (MALII binding) was observed with any treatment, consistent with Fig. 1. To determine if this result led to altered N-glycoforms of ICAM-1 on the cell surface, we utilized the proximity ligation assay (PLA). Fig. 4B and C shows TNFα-treated ECs increased both HM-ICAM-1 and α-2,6-sialyated ICAM-1; PEG-catalase however only inhibited expression of HM-ICAM-1. Our previous studies validated that these PLA signals represent ICAM-1 N-glycoform on the cell surface and that HM-ICAM-1 selectively mediates adhesion of $CD16^+$ monocytes, but has no role in adhering to $CD16^-$ monocytes [15]. Fig. 4D shows that TNFα treatment of ECs increase adhesion of both monocyte subsets. PEG-catalase partially inhibited $CD16^-$

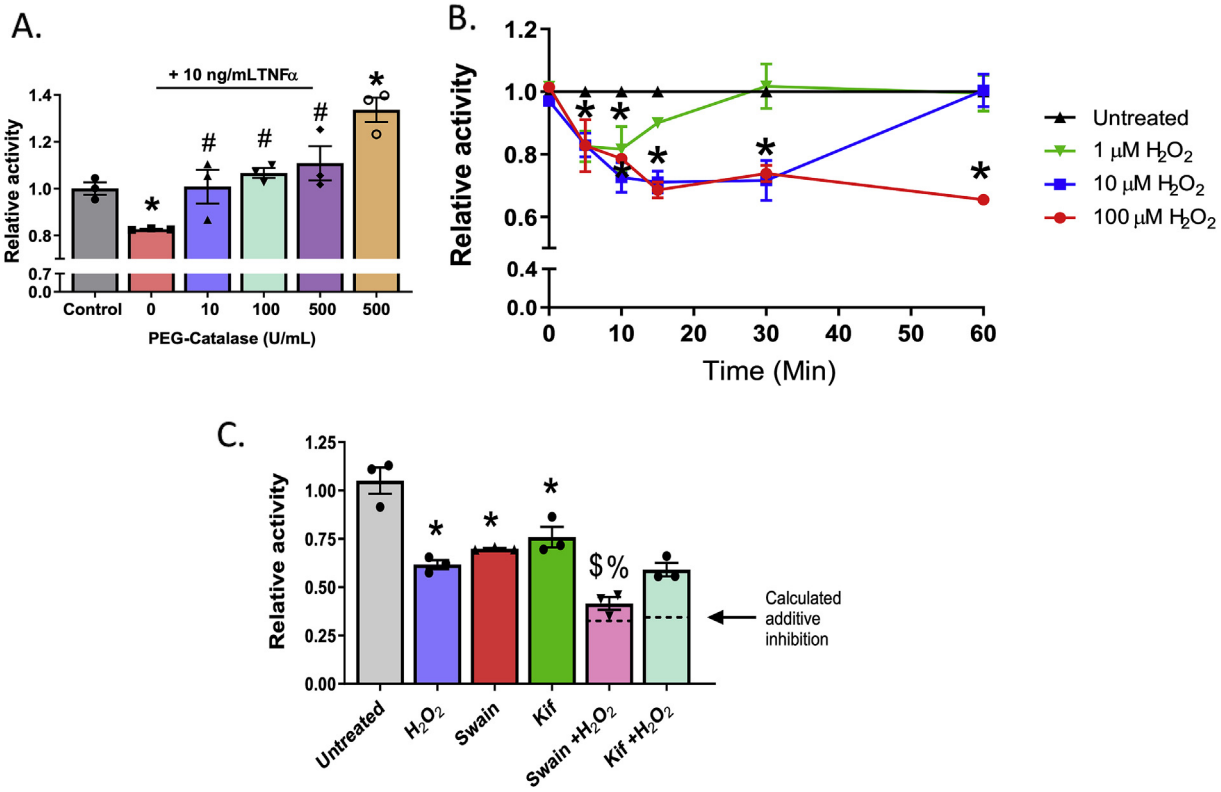

Fig. 3. Hydrogen peroxide inhibits α-mannosidase activity in a time and dose dependent manner. A. HUVECs were pre-treated with increasing doses of PEG-Catalase for 30 min prior to TNFα treatment and α-mannosidase activity measured. * = $p \leq 0.05$ compared to untreated control. # = $p \leq 0.05$ compared to TNFα alone by 1-way ANOVA with Tukey post-test. Data are mean ± SEM, n = 3. **B.** HUVECs were treated with 0, 1, 10, or 100 μM exogenous H_2O_2 for increments between 0 and 60 min and α-mannosidase activity measured. * = $p \leq 0.05$ compared to untreated control by 1-way ANOVA with Tukey post-test. Data are mean ± SEM, n = 3. **C.** HUVECs were pretreated with Kif or Swain 2 h prior to 100 μM H_2O_2 treatment for 1 h and α-mannosidase activity measured. Dotted lines represent calculated additive effect determined by level of inhibition from H_2O_2 combined with inhibition of Kif alone or Swain alone as described in results section. * = $p \leq 0.05$ compared to untreated control; $ = $p \leq 0.05$ compared to Swain; & = $p \leq 0.05$ compared to H_2O_2 by 1-way ANOVA with Tukey post-test. Data are mean ± SEM, n = 3.

monocyte adhesion, but completely attenuated $CD16^+$ monocyte rolling and adhesion. PEG-catalase treatment alone had no effect. Similarly, TNFα treatment of ECs decreased velocities of both monocyte subsets, with PEG-catalase preventing this with $CD16^+$ monocytes only (Fig. 4E). Importantly, these effects on rolling and adhesion associated with N-glycoforms of ICAM-1 and not changes in surface levels of the ICAM-1 protein itself (Fig. 4F).

3.5. Inhibition of ERO1-α rescues TNFα inhibition of α-mannosidase activity

After establishing that H_2O_2 modulates α-mannosidase activity, we then wanted to determine where the H_2O_2 was originating from during TNFα treatment. Because some of these α-mannosidases reside in the ER, we first tested H_2O_2-producing enzymes in the ER: NADPH-oxidase 4 (NOX4) and ERO1α [31] The effects of the dual NOX1/4 inhibitor GKT137831 [32], and the ERO1α inhibitor EN460 [33] were tested. Fig. 5A shows that NOX4 inhibition had no effect on α-mannosidase activity, while inhibiting ERO1α reversed the effect of TNFα, suggesting that the source of H_2O_2 via TNFα is the latter. ERO1α accepts electrons from reduced protein disulfide isomerase, which in turn modulates disulfide formation during protein translation. The reduced ERO1 is re-oxidized by molecular oxygen, the latter being reduced to H_2O_2 in the ER [31,34]. EN460 is a small-molecule inhibitor that binds reduced ERO1α preventing its oxidation and H_2O_2 production [33]. The oxidized and reduced forms of ERO1α can be monitored by their differential migration on a non-reducing Western blot [33]. Fig. 5B shows that under basal (steady state) conditions, ~5–10% of ERO1α is in the reduced state. After TNFα treatment however, total levels of ERO1α increased ~3-fold with the proportion of the reduced form increasing to ~25%. EN460 treatment alone increased the proportion of reduced ERO1α to ~40%. Importantly, EN460 did not change TNFα-dependent increased expression of ERO1α, but did further increase the proportion that was reduced to ~50%. Fig. 5C shows that EN460 inhibited TNFα dependent increases in DCF fluorescence also, demonstrating a role for ERO1α derived DCF-reactive species in ECs stimulated with TNFα. Fig. 5D shows ERO1α inhibition decreased HM-N-glycan expression on the cell surface but not of α-2,6-sialyated N-glycans. Fig. 5E and F shows representative PLA images and quantitation of HM- and α-2,6-sialyated ICAM-1; EN460 treatment abrogates TNFα induced HM-ICAM-1 but not complex ICAM-1. Consistent with these observations, inhibition of ERO1α selectively inhibited $CD16^+$ monocyte adhesion to TNFα-treated ECs under flow, but had no effect on $CD16^-$ monocyte adhesion (Fig. 5G). Importantly, these effects were not due to altered levels of ICAM-1 protein on the cell surface (Fig. 5H).

4. Discussion

N-glycosylation regulates protein function in multiple ways including ensuring correct folding, trafficking to the surface or extracellular compartment, modulating protein stability, conformation and providing ligands that mediate cell-cell interactions. Our recent study suggest that HM structures on ICAM-1 provide ligands to selectively recruit pro-inflammatory ($CD16^+$) monocytes; a subset that strongly associates with increased risk and more severe cardiovascular disease [17–19]. In this study, we demonstrate that one mechanism for HM-

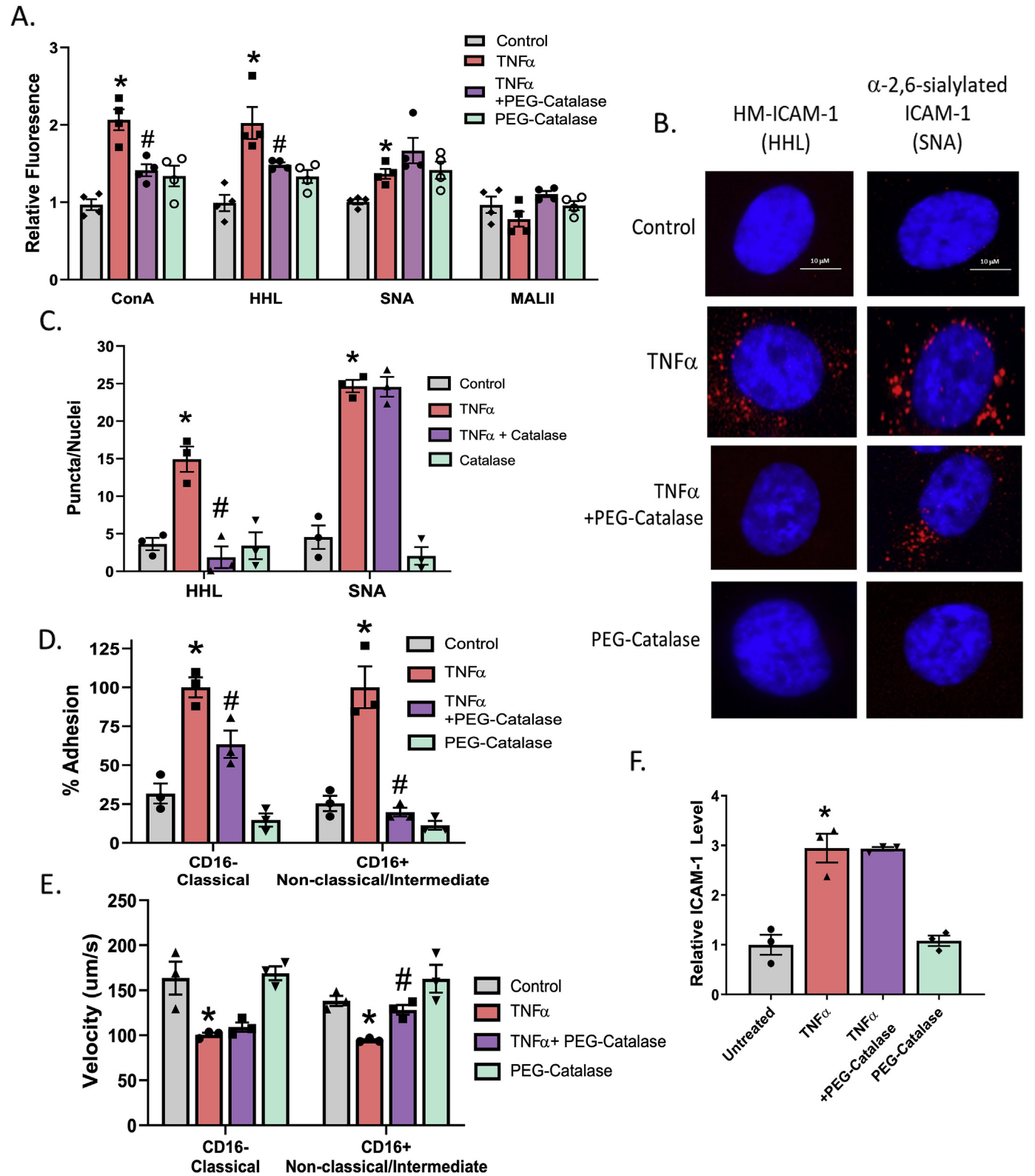

Fig. 4. TNFα-induced HM-ICAM-1 formation and α-mannosidase activity inhibition can be reversed with PEG-Catalase. A. HUVECs treated with 100 units of PEG-catalase 30 min prior to TNFα treatment and lectin staining with ConA, HHL, SNA, and MAL-II was performed. * = $p \leq 0.05$ compared to control; # = $p \leq 0.05$ compared to TNFα by 1-way ANOVA with Tukey post-test. Data are mean ± SEM, n = 3 **B.** HUVECs were treated as described in **A** and subject to proximity-ligation assay (PLA) for HM- (HHL) and α-2,6,-sialylated (SNA) ICAM-1. Shown are representative images. Red puncta indicate positive staining for the ICAM-1 N-glycoform probed. **C.** Quantitation of red puncta from panel B. * = $p < 0.05$ compared to control; # = $p \leq 0.05$ compared to TNFα by 1-way ANOVA with Tukey post-test. Data are mean ± SEM, n = 3. **D.** HUVECs were treated as described above and $CD16^-$ and $CD16^+$ monocyte adhesion to the ECs was measured under flow. * = $p < 0.05$ compared to control; # = $p \leq 0.05$ compared to TNFα by 1-way ANOVA with Tukey post-test. Data are mean ± SEM, n = 3. **E.** Monocyte rolling velocities calculated from (D). Data are mean ± SEM, n = 3. * = $p < 0.05$ compared to control; # = $p \leq 0.05$ compared to TNFα by 1-way ANOVA with Tukey post-test. **F.** HUVECs were treated as described above and total surface ICAM-1 was measured via ELISA. * = $p < 0.05$ compared to control by 1-way ANOVA with Tukey post-test. Data are mean ± SEM, n = 3. (For interpretation of the references to colour in this figure legend, the reader is referred to the Web version of this

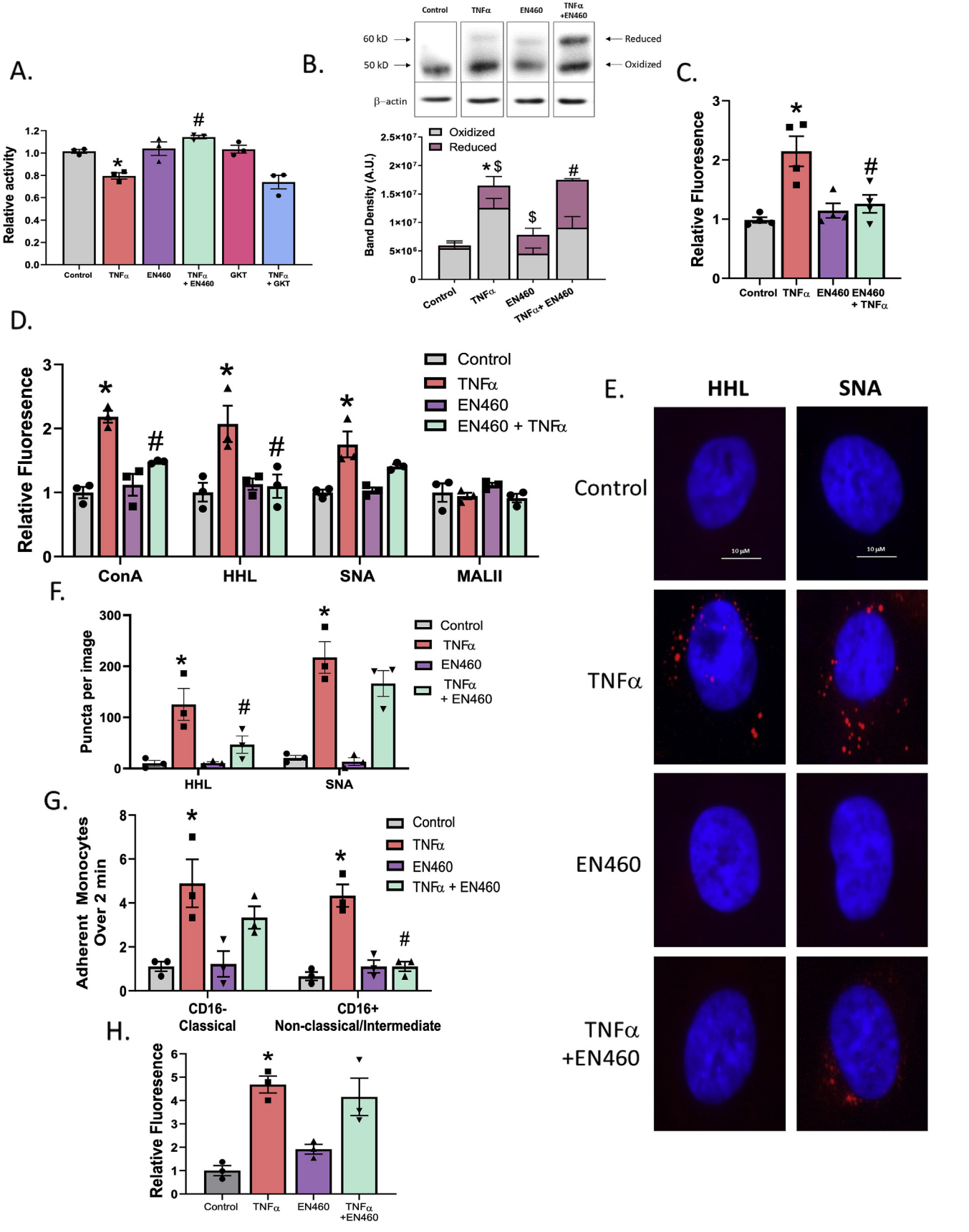

(caption on next page)

Fig. 5. ERO1-α inhibition abrogates TNFα-inhibition of α mannosidase activity and HM N-glycan formation. A. HUVECs were pretreated with either 10 μM GKT137831 or 5 μM EN460 to inhibit NOX4, ERO1-α, respectively, prior to TNFα treatment and α-mannosidase activity measured. * = p ≤ 0.05 compared to control; # = p ≤ 0.05 compared to TNFα by 1-way ANOVA with Tukey post-test. Data are mean ± SEM, n = 3. **B.** HUVECs were treated with 5 μM EN460 to inhibit ERO1-α prior to TNFα and oxidized and reduced ERO1α measured via Western blot. Data are mean ± SEM, n = 3. * = p ≤ 0.05 total ERO1α levels compared to control; # = p ≤ 0.05 reduced form compared to TNFα; $ = p ≤ 0.05 reduced form compared to control by 1-way ANOVA with Tukey post-test. **C.** ROS measurement by DCF assay in HUVECs treated as described above. Data are mean ± SEM, n = 3. * = p ≤ 0.05 compared to control; # = p ≤ 0.05 compared to TNFα by 1-way ANOVA with Tukey post-test. **D.** Four lectin stains of HUVECs treated with TNFα and EN460. * = p ≤ 0.05 compared to control; # = p ≤ 0.05 compared to TNFα by 1-way ANOVA with Tukey post-test. **E.** Representative images of HUVECs treated as described above and subject to PLA for HM- and α-2,6,-sialylated ICAM-1 via HHL and SNA. Red puncta indicate positive staining for the ICAM-1 N-glycoform probed. **F.** PLA quantitation. * = p ≤ 0.05 compared to control; # = p ≤ 0.05 compared to TNFα by 1-way ANOVA with Tukey post-test. Data are mean ± SEM, n = 3. **G.** HUVECs were treated as described and $CD16^-$ and $CD16^+$ monocyte adhesion to the ECs was measured under flow. * = p ≤ 0.05 compared to control; # = p ≤ 0.05 compared to TNFα by 1-way ANOVA with Tukey post-test. Data are mean ± SEM, n = 3. **H.** HUVECs were treated as described and surface ICAM-1 was measured via ELISA. * = p ≤ 0.05 compared to control by 1-way ANOVA with Tukey post-test. Data are mean ± SEM, n = 3. (For interpretation of the references to colour in this figure legend, the reader is referred to the Web version of this article.)

ICAM-1 formation is inhibition of α-mannosidase, and further identify ER-derived H_2O_2 as an important mediator of this inhibition.

Our previous work showed that TNFα decreases α-mannosidase activity in endothelial cells [26]. We extend this understanding to show that TNFα specifically inhibits class I α-mannosidases. There are 4 class I and 5 class II α-mannosidase isoforms, however their relative protein expression and activities in ECs is not known. A further limitation is the lack of methods that discern isoform specific activity. The method we employed to measure α-mannosidase activity measures both class I and II isoforms. Notwithstanding method limitations, we used two well characterized inhibitors of class I and II α-mannosidases and based on the lack of additive inhibition with TNFα or H_2O_2 with Kif, we conclude that class I α-mannosidases are inhibited by TNFα or H_2O_2. We speculate that the ~25–30% inhibition observed with TNFα, or low dose H_2O_2, reflects inhibition of a small subset of the four class I α-mannosidases. Ongoing studies will determine which class I isoform(s) are important, but to our knowledge, this is the first report of a class of α-mannosidases being subject to redox-dependent modulation.

Another important observation was that inhibition of α-mannosidase activity in EC *in vitro* was transient and paralleled transient increases in surface HM-ICAM-1. This may reflect a response more typical of innate immunity where HM-ICAM1 increases and then decreases to allow resolution of acute inflammation to occur. Also of note, it was only in HUVEC and HAEC where α-mannosidase activity decreased and HM epitopes increased; PMVECs had an increase only in α-2,3-sialylation. These data also provide a potential mechanism that underlies functional heterogeneity in endothelial cells from different vascular beds and support our hypothesis of an N-glycan endothelial "zip-code" for the selective recruitment of monocytes to sites prone to chronic vascular inflammatory disease [5,35,36].

One of the major effects of TNFα on endothelial cells is the production of H_2O_2 [37–39], which led us to test a role for this reactive species in modulating α-mannosidase activity. Attenuation of TNFα effects by PEG-catalase, and replication of α-mannosidase inhibition by reagent H_2O_2 identifies, to our knowledge, a novel role for reactive species in regulating protein N-glycosylation. While there are studies documenting the association between reactive species and advanced glycation end products, potential links between redox signaling and N-glycosylation have only been hypothesized to date [40–42]. A common feature in redox signaling is altered activity of kinases and phosphatases and ensuring changes in protein phosphorylation. Presented data extend these paradigms to include regulation of α-mannosidase activity and modulation of protein N-glycoforms. Given that N-glycosylation occurs on > 60% of cell-surface and secreted proteins [1], we speculate that ER-redox homeostasis will play important roles in regulating the function of proteins that are secreted or expressed on the cell surface.

H_2O_2 inhibited α-mannosidase activity within 15 min and at relatively low doses (1–10 μM) when administered exogenously. While we have not quantified H_2O_2 levels in the ER in TNFα or H_2O_2 treated cells, this result suggests effects of H_2O_2 are potent and likely via direct modifications to the α-mannosidase(s) themselves. Our working hypothesis is that H_2O_2 reacts with one or more of the 4 class I α-mannosidases, inducing an oxidative-post-translational modification that results in inhibition or rapid protein degradation, rather than inhibition of gene-transcription. Notably, activity returned to baseline relatively quickly (30min) consistent with an oxidative- and reversible post-translational modification mechanism.

There are multiple potential sources of H_2O_2 in ECs. The ER contains both H_2O_2 producing enzymes and antioxidant systems, including GPX7/8, Prx 4 and a dynamic glutathione pool; for example, Anathy, et al. showed that ER-produced H_2O_2 mediates S-glutathionylation of Fas ligand to regulate apoptosis [43]. Such data underscore the potential for the ER to be a redox signaling hub within the cell [44–49]. Other groups have studied how oxidant and antioxidant systems play roles in ER redox homeostasis in various organ systems such as the CNS neurons and hepatocytes [50,51]. However, relatively little is known about ER-dependent mechanisms and regulation of redox signaling in ECs. Since the majority of α-mannosidases reside in the ER-Golgi secretory pathway, we focused on H_2O_2-producing enzymes in this compartment. Our data identified ERO1α as a target of TNFα dependent activation of ECs and the source of H_2O_2 that regulates protein N-glycosylation. Whether increases in ERO1α represents an integrated response of the ER to upregulated protein transcription and translation or a selective effect of TNFα on ERO1α specifically remains to be determined. Similarly, further studies need to evaluate whether this is a general response to inflammatory stimuli or specific to TNFα. We also note the limitation that while our data support a role for ERO1α, further studies are needed to exclude NOX4 (recent studies have shown that the NOX4 inhibitor used may have other non-specific effects [32,52]) and test other cellular sources of H_2O_2.

In summary, the data herein provide evidence for a novel redox signaling mechanism, whereby ER-H_2O_2 modulates formation of protein N-glycoforms, further underscoring the role of ER-redox homeostasis and control of the surface and secreted proteome.

Declaration of competing interest

The authors declare no conflicts of interest.

Acknowledgments

This study was supported by T32 HL007918 (KRM), and T32 GM109780 (AHN), and the K99/R00 Pathway to Independence Award R00HL131866 (J.W.B.).

Appendix A. Supplementary data

Supplementary data to this article can be found online at https://doi.org/10.1016/j.redox.2020.101498.

References

[1] P. Stanley, H. Schachter, N. Taniguchi, N-Glycans, nd, A. Varki, R.D. Cummings, J.D. Esko, H.H. Freeze, P. Stanley, C.R. Bertozzi, G.W. Hart, M.E. Etzler (Eds.), Essentials of Glycobiology, Cold Spring Harbor, (NY), 2009.

[2] M. Aebi, N-linked protein glycosylation in the ER, Biochim. Biophys. Acta 1833 (2013) 2430–2437.

[3] J. Breitling, M. Aebi, N-linked protein glycosylation in the endoplasmic reticulum, Cold Spring Harb. Perspect. Biol. 5 (2013) a013359.

[4] E. Galkina, K. Ley, Immune and inflammatory mechanisms of atherosclerosis (*), Annu. Rev. Immunol. 27 (2009) 165–197.

[5] J. Renkonen, O. Tynninen, P. Hayry, T. Paavonen, R. Renkonen, Glycosylation might provide endothelial zip codes for organ-specific leukocyte traffic into inflammatory sites, Am. J. Pathol. 161 (2002) 543–550.

[6] J.W. Dennis, M. Granovsky, C.E. Warren, Protein glycosylation in development and disease, Bioessays 21 (1999) 412–421.

[7] B.K. Chacko, D. Scott, R.T. Chandler, R.P. Patel, Endothelial surface N-Glycans mediate monocyte adhesion and are targets for anti-inflammatory effects of peroxisome proliferator-activated receptor Y ligands, J. Biol. Chem. 286 (2011) 38738–38747.

[8] J.J. Garcia-Vallejo, W. Van Dijk, B. Van Het Hof, I. Van Die, M.A. Engelse, V.W. Van Hinsbergh, S.I. Gringhuis, Activation of human endothelial cells by tumor necrosis factor-alpha results in profound changes in the expression of glycosylation-related genes, J. Cell. Physiol. 206 (2006) 203–210.

[9] A. Kobata, J. Amano, Altered glycosylation of proteins produced by malignant cells, and application for the diagnosis and immunotherapy of tumours, Immunol. Cell Biol. 83 (2005) 429–439.

[10] D. Scott, T. Dunn, M. Ballestas, S. Litovsky, R.P. Patel, Identification of a high-mannose ICAM-1 glycoform: effects of ICAM-1 hypoglycosylation on monocyte adhesion and outside in signaling, Am. J. Physiol. Cell Physiol. 305 (2013) C228–C237.

[11] D.O. Croci, J.P. Cerliani, T. Dalotto-Moreno, S.P. Mendez-Huergo, I.D. Mascanfroni, S. Dergan-Dylon, M.A. Toscano, J.J. Caramelo, J.J. Garcia-Vallejo, J. Ouyang, E.A. Mesri, M.R. Junttila, C. Bais, M.A. Shipp, M. Salatino, G.A. Rabinovich, Glycosylation-dependent lectin-receptor interactions preserve angiogenesis in anti-VEGF refractory tumors, Cell 156 (2014) 744–758.

[12] S.R. Stowell, T. Ju, R.D. Cummings, Protein glycosylation in cancer, Annu. Rev. Pathol. 10 (2015) 473–510.

[13] M.L. de Leoz, L.J. Young, H.J. An, S.R. Kronewitter, J. Kim, S. Miyamoto, A.D. Borowsky, H.K. Chew, C.B. Lebrilla, High-mannose glycans are elevated during breast cancer progression, Mol. Cell. Proteomics 10 (2011) M110 002717.

[14] K. Talabnin, C. Talabnin, M. Ishihara, P. Azadi, Increased expression of the high-mannose M6N2 and NeuAc3H3N3M3N2F tri-antennary N-glycans in cholangiocarcinoma, Oncol. Lett. 15 (2018) 1030–1036.

[15] K. Regal-McDonald, B. Xu, J.W. Barnes, R.P. Patel, High-mannose intercellular adhesion molecule-1 enhances CD16(+) monocyte adhesion to the endothelium, Am. J. Physiol. Heart Circ. Physiol. 317 (2019) H1028–H1038.

[16] D.W. Scott, J. Chen, B.K. Chacko, J.G. Traylor, A.W. Orr, R.P. Patel, Role for endothelial N-glycan mannose residues in monocyte recruitment during atherogenesis, Arterioscler. Thromb. Vasc. Biol. 32 (2012).

[17] M. Wildgruber, M. Czubba, T. Aschenbrenner, H. Wendorff, A. Hapfelmeier, A. Glinzer, M. Schiemann, A. Zimmermann, H.H. Eckstein, H. Berger, W.A. Wohlgemuth, R. Meier, P. Libby, A. Zernecke, Increased intermediate CD14(++)CD16(++) monocyte subset levels associate with restenosis after peripheral percutaneous transluminal angioplasty, Atherosclerosis 253 (2016) 128–134.

[18] M. Wildgruber, T. Aschenbrenner, H. Wendorff, M. Czubba, A. Glinzer, B. Haller, M. Schiemann, A. Zimmermann, H. Berger, H.H. Eckstein, R. Meier, W.A. Wohlgemuth, P. Libby, A. Zernecke, The "Intermediate" CD14(++)CD16(+) monocyte subset increases in severe peripheral artery disease in humans, Sci. Rep. 6 (2016) 39483.

[19] K.S. Rogacev, B. Cremers, A.M. Zawada, S. Seiler, N. Binder, P. Ege, G. Grosse-Dunker, I. Heisel, F. Hornof, J. Jeken, N.M. Rebling, C. Ulrich, B. Scheller, M. Bohm, D. Fliser, G.H. Heine, CD14++CD16+ monocytes independently predict cardiovascular events: a cohort study of 951 patients referred for elective coronary angiography, J. Am. Coll. Cardiol. 60 (2012) 1512–1520.

[20] K. Fujiyama, S. Sakuradani, D.G. Moran, T. Yoshida, T. Seki, Effect of alpha1,2-mannosidic linkage located in a alpha1,3-branch of Man6GlcNAc2 oligosaccharide on enzyme activity of recombinant human Man9-mannosidase produced in Escherichia coli, J. Biosci. Bioeng. 91 (2001) 419–421.

[21] J. Isoyama-Tanaka, K. Dohi, R. Misaki, K. Fujiyama, Improved expression and characterization of recombinant human Golgi alpha1,2-mannosidase I isoforms (IA2 and IC) by Escherichia coli, J. Biosci. Bioeng. 112 (2011) 14–19.

[22] F. Lipari, B.J. Gour-Salin, A. Herscovics, The Saccharomyces cerevisiae processing alpha 1,2-mannosidase is an inverting glycosidase, Biochem. Biophys. Res. Commun. 209 (1995) 322–326.

[23] N. Shah, D.A. Kuntz, D.R. Rose, Comparison of kifunensine and 1-deoxymannojirimycin binding to class I and II alpha-mannosidases demonstrates different saccharide distortions in inverting and retaining catalytic mechanisms, Biochemistry 42 (2003) 13812–13816.

[24] A. Herscovics, Structure and function of Class I alpha 1,2-mannosidases involved in glycoprotein synthesis and endoplasmic reticulum quality control, Biochimie 83 (2001) 757–762.

[25] N. Shah, D.A. Kuntz, D.R. Rose, Golgi alpha-mannosidase II cleaves two sugars sequentially in the same catalytic site, Proc. Natl. Acad. Sci. U. S. A. 105 (2008) 9570–9575.

[26] D.W. Scott, M.O. Vallejo, R.P. Patel, Heterogenic endothelial responses to inflammation: role for differentital N-glycosylation and vascular bed of origin, J. Am. Heart Assoc. 2 (2013) e000263.

[27] C.G. Kevil, R.P. Patel, D.C. Bullard, Essential role of ICAM-1 in mediating monocyte adhesion to aortic endothelial cells, Am. J. Physiol. Cell Physiol. 281 (2001) C1442–C1447.

[28] R.J. Esper, R.A. Nordaby, J.O. Vilarino, A. Paragano, J.L. Cacharron, R.A. Machado, Endothelial dysfunction: a comprehensive appraisal, Cardiovasc. Diabetol. 5 (2006) 4.

[29] M.P. Bevilacqua, Endothelial-leukocyte adhesion molecules, Annu. Rev. Immunol. 11 (1993) 767–804.

[30] P.P. Tak, G.S. Firestein, NF-kappaB: a key role in inflammatory diseases, J. Clin. Invest. 107 (2001) 7–11.

[31] C.S. Sevier, C.A. Kaiser, Ero1 and redox homeostasis in the endoplasmic reticulum, Biochim. Biophys. Acta 1783 (2008) 549–556.

[32] F. Gaggini, B. Laleu, M. Orchard, L. Fioraso-Cartier, L. Cagnon, S. Houngninou-Molango, A. Gradia, G. Duboux, C. Merlot, F. Heitz, C. Szyndralewiez, P. Page, Design, synthesis and biological activity of original pyrazolo-pyrido-diazepine, -pyrazine and -oxazine dione derivatives as novel dual Nox4/Nox1 inhibitors, Bioorg. Med. Chem. 19 (2011) 6989–6999.

[33] J.D. Blais, K.T. Chin, E. Zito, Y. Zhang, N. Heldman, H.P. Harding, D. Fass, C. Thorpe, D. Ron, A small molecule inhibitor of endoplasmic reticulum oxidation 1 (ERO1) with selectively reversible thiol reactivity, J. Biol. Chem. 285 (2010) 20993–21003.

[34] K. Araki, S. Iemura, Y. Kamiya, D. Ron, K. Kato, T. Natsume, K. Nagata, Ero1-alpha and PDIs constitute a hierarchical electron transfer network of endoplasmic reticulum oxidoreductases, J. Cell Biol. 202 (2013) 861–874.

[35] P.E. Thorpe, S. Ran, Mapping zip codes in human vasculature, Pharmacogenomics J. 2 (2002) 205–206.

[36] K. Regal-McDonald, R.P. Patel, Sweet and sticky: selective recruitment of monocyte subsets by endothelial N-glycans, Am. J. Pathol. (2020), https://doi.org/10.1016/j.ajpath.2020.01.006 In Press. PMID: 32084367.

[37] X. Chen, B.T. Andresen, M. Hill, J. Zhang, F. Booth, C. Zhang, Role of reactive oxygen species in tumor necrosis factor-alpha induced endothelial dysfunction, Curr. Hypertens. Rev. 4 (2008) 245–255.

[38] C.H. Woo, Y.W. Eom, M.H. Yoo, H.J. You, H.J. Han, W.K. Song, Y.J. Yoo, J.S. Chun, J.H. Kim, Tumor necrosis factor-alpha generates reactive oxygen species via a cytosolic phospholipase A2-linked cascade, J. Biol. Chem. 275 (2000) 32357–32362.

[39] C.N. Young, J.I. Koepke, L.J. Terlecky, M.S. Borkin, L. Boyd Savoy, S.R. Terlecky, Reactive oxygen species in tumor necrosis factor-alpha-activated primary human keratinocytes: implications for psoriasis and inflammatory skin disease, J. Invest. Dermatol. 128 (2008) 2606–2614.

[40] D. Yao, M. Brownlee, Hyperglycemia-induced reactive oxygen species increase expression of the receptor for advanced glycation end products (RAGE) and RAGE ligands, Diabetes 59 (2010) 249–255.

[41] K. Nowotny, T. Jung, A. Hohn, D. Weber, T. Grune, Advanced glycation end products and oxidative stress in type 2 diabetes mellitus, Biomolecules 5 (2015) 194–222.

[42] N. Taniguchi, Y. Kizuka, S. Takamatsu, E. Miyoshi, C. Gao, K. Suzuki, S. Kitazume, K. Ohtsubo, Glyco-redox, a link between oxidative stress and changes of glycans: lessons from research on glutathione, reactive oxygen and nitrogen species to glycobiology, Arch. Biochem. Biophys. 595 (2016) 72–80.

[43] V. Anathy, E. Roberson, B. Cunniff, J.D. Nolin, S. Hoffman, P. Spiess, A.S. Guala, K.G. Lahue, D. Goldman, S. Flemer, A. van der Vliet, N.H. Heintz, R.C. Budd, K.D. Tew, Y.M. Janssen-Heininger, Oxidative processing of latent Fas in the endoplasmic reticulum controls the strength of apoptosis, Mol. Cell Biol. 32 (2012) 3464–3478.

[44] Y.M. Kim, S.J. Kim, R. Tatsunami, H. Yamamura, T. Fukai, M. Ushio-Fukai, ROS-induced ROS release orchestrated by Nox4, Nox2, and mitochondria in VEGF signaling and angiogenesis, Am. J. Physiol. Cell Physiol. 312 (2017) C749–C764.

[45] L.B. Poole, C. Schoneich, Introduction: what we do and do not know regarding redox processes of thiols in signaling pathways, Free Radic. Biol. Med. 80 (2015) 145–147.

[46] T. Ramming, C. Appenzeller-Herzog, Destroy and exploit: catalyzed removal of hydroperoxides from the endoplasmic reticulum, Int. J. Cell Biol. 2013 (2013) 180906.

[47] Y. Sato, R. Kojima, M. Okumura, M. Hagiwara, S. Masui, K. Maegawa, M. Saiki, T. Horibe, M. Suzuki, K. Inaba, Synergistic cooperation of PDI family members in peroxiredoxin 4-driven oxidative protein folding, Sci. Rep. 3 (2013) 2456.

[48] L. Wang, L. Zhang, Y. Niu, R. Sitia, C.C. Wang, Glutathione peroxidase 7 utilizes hydrogen peroxide generated by Ero1alpha to promote oxidative protein folding, Antioxidants Redox Signal. 20 (2014) 545–556.

[49] S. Kim, D.P. Sideris, C.S. Sevier, C.A. Kaiser, Balanced Ero1 activation and inactivation establishes ER redox homeostasis, J. Cell Biol. 196 (2012) 713–725.

[50] M. Mari, A. Colell, A. Morales, C. von Montfort, C. Garcia-Ruiz, J.C. Fernandez-Checa, Redox control of liver function in health and disease, Antioxidants Redox Signal. 12 (2010) 1295–1331.

[51] X. Ren, L. Zou, X. Zhang, V. Branco, J. Wang, C. Carvalho, A. Holmgren, J. Lu, Redox signaling mediated by thioredoxin and glutathione systems in the central nervous system, Antioxidants Redox Signal. 27 (2017) 989–1010.

[52] S. Altenhofer, K.A. Radermacher, P.W. Kleikers, K. Wingler, H.H. Schmidt, Evolution of NADPH oxidase inhibitors: selectivity and mechanisms for target engagement, Antioxidants Redox Signal. 23 (2015) 406–427.